



# Kinetics, Isotherms, and Thermodynamics Studies on Adsorption of Methyl Green Dye Onto Different Zeolites

Fatma A. Ibrahim<sup>1</sup> · Amal A. Atran<sup>1</sup> · Mohamed S. Hamdy<sup>1</sup>

Received: 28 September 2023 / Accepted: 21 December 2023

© The Author(s), under exclusive licence to Springer Science+Business Media, LLC, part of Springer Nature 2024

## Abstract

The adsorption of methyl green (MG) dye from aqueous solutions over different zeolite samples was investigated. Five types of zeolites H-Y (HY), H-BETA (Beta), NH<sub>4</sub>-Mordenite (MOR), NH<sub>4</sub>-ZSM-5 (ZSM-5), and NH<sub>4</sub>-Ferrierite (FERR) were obtained and characterized by X-Ray diffraction analysis (XRD), Fourier transform infrared spectroscopy (FTIR), inductively coupled plasma (ICP) elemental analysis, N<sub>2</sub> sorption measurements, and scanning electron microscopy (SEM). The obtained characterization results pointed out to several significant differences between the investigated samples such as morphological structure, textural properties, aluminium content, and the counter cation. The adsorption capacities of HY, Beta, and MOR zeolites using MG were determined to be 41.54, 25.05 mg/g, and 40.57, respectively. On the other hand, FERR and ZSM-5 exhibited the smallest adsorption capacity. The process of adsorption was optimized in terms of a number of variables, including contact time, adsorbent dosage, solution pH, dye concentration, and solution temperature. Moreover, the kinetics, isotherm, and thermodynamic parameters of adsorption were calculated. The Langmuir isotherm model had the best correlation with the experimental data, and the kinetics studies showed that the adsorption followed pseudo-second order kinetics. Moreover, the mechanism of adsorption process was proposed and discussed.

**Keywords** Zeolites · Adsorption · Methyl green · Kinetics · Langmuir

## 1 Introduction

As a result of increasing the human industrial activities, several pollutants are released continuously to air, water streams and soil [1]. These contaminations are considered a real thread to the environment and can create several health problems to human in addition to the other to the ecological life [2]. Organic dyes are one of the most common contaminants found in wastewater [3]. Dyes are released to the water streams from textile, food, dyeing, painting and other industries [4]. Dyes have a significant environmental impact, in which 1 ppm of some dyes can change the colour of water streams which makes it unusable [5]. Furthermore, cationic dyes have been found to be more harmful than anionic dyes [6]. The removal of dye from wastewater is a major ecological issue around the

world. There are several techniques for removing organic dyes, which including ozonation, aerobic treatment, biodegradation [7], oxidative catalytic degradation [8], coagulation [9], electrochemical degradation [10], membrane separation [11], and adsorption techniques [12–15]. One of the most common methods for removing organic dyes is adsorption, since it is simple, easy, cost-effective, efficient, and safe. MG is one of the dyes, which is applying on a large scale in several industries such as colouring of textile [16], plastic, and leather [17]. MG also has some applications in medicine, gelatine film awareness, and biological applications [18–20]. However, there are some health issues regarding the use of MG dye, because it was reported that it can cause severe skin burns and eye damage, therefore, the removal of this dye from water streams is crucial. Several studies were reported about the removal of MG dye from water streams. Belmedani et al. [21] reported the removal of MG dye from aqueous solutions by using activated carbon as a strong adsorbent in a spontaneous exothermic process. In another study, Mahmoud et al. [22] investigated the same target by using hydrated zinc oxide doped silica gel by. Moreover, Charaf

✉ Mohamed S. Hamdy  
m.s.hamdy@gmail.com

<sup>1</sup> Catalysis Research Group (CRG), Department of Chemistry, College of Science, King Khalid University, PO Box 9004, 61413 Abha, Saudi Arabia

et al. [23] utilized the Sejnane clay as an adsorbent for MG. It has been reported that the adsorption process is endothermic and spontaneous chemisorption process. Finally, Hamdy et al. [24] reported the use of modified three-dimensional mesoporous silica to adsorb MG. The reported results showed that the adsorption capacity has improved from 15 mg/g for neat silica to 248 mg/g for the modified mesoporous silica.

Zeolites are a distinct class of solid materials with numerous applications in industrial processes and pollution management. Zeolites are hydrated aluminosilicate minerals with a polyhedral three-dimensional framework based on  $[\text{SiO}_4]$  and  $[\text{AlO}_5]$  compounds, which can be found in both natural and synthetic types. These compounds are joined to one another by their oxygens, forming a regular network of interconnecting pores and tunnels [25]. Zeolites have a unique structure and properties that enable excellent adsorption of a variety of pollutants in the environment. In addition, zeolite has a large surface area, which is a critical feature for adsorbents. Natural zeolite has a surface area around 20–50  $\text{m}^2/\text{g}$ , however, the surface area of synthetic zeolite can reach 1000  $\text{m}^2/\text{g}$ . Zeolites have intracrystalline voids account for 20–50 percent of its total crystal volume in most types [26, 27]. According to international zeolite association (IZA), there are more than 150 types of zeolites were fabricated with different features such as morphological and textural properties and Al content. Many zeolites types are commercialized and are applying in several applications such as adsorption, dehydration, and catalysis [28]. Zeolite was perfectly applied as a sorbent material for many pollutants such as heavy metals and dyes. Cravotto et al. [29] reported the use of modified zeolite Y for the removal of methylene blue dye. It was reported that the modified zeolite with its high adsorption capacity is stable for the consecutive four runs. In another study, Mouni et al. [30] used 4A zeolite in the removal of malachite green dye, and it was reported that the process is a spontaneous endothermic process. Ginting et al. reported the use of modified zeolite-iron chloride for the removal of Cr(VI), while Sarangi et al. [31] reported the use of Zeolite X in the removal of  $\text{Cd}^{2+}$  and  $\text{Zn}^{2+}$ . Finally, Ibrahim et al. [15] reported the adsorption behaviour of home-made zeolite, entitled "black zeolite". The prepared material exhibited high adsorption behaviour in the removal of methylene blue dye from an aqueous solution.

To the best of the available knowledge, there is no systematic study for the removal of MG dye over different zeolites. In the current study, the research team compared -for the first time- the adsorption behaviour of five types of commercially available zeolites (HY, Beta, MOR, ZSM-5, and FERR) in the removal of MG, as a model cationic dye, from aqueous solution under several conditions. The thermodynamic parameters as well as the kinetics of the removal process are reported and discussed.

## 2 Experimental

### 2.1 Chemicals

Methyl green ( $\text{C}_{26}\text{H}_{33}\text{Cl}_2\text{N}_3$ ) was selected as cationic dye and it was purchased from VWR Chemicals BDH®, Atlanta, USA. Hydrochloric acid (HCl, 37%) and sodium hydroxide (NaOH, 98%) were obtained from Sigma-Aldrich®, Darmstadt, Germany. The investigated zeolites H-Y, H-Beta,  $\text{NH}_4$ -Mordenite,  $\text{NH}_4$ -ZSM-5 and  $\text{NH}_4$ -Ferrierite were purchased from Zeolyst®, Pennsylvania, USA. The obtained zeolite samples are coded as HY, Beta, MOR, ZSM-5, and FERR; respectively. These codes will be fixed in the entire study. The entire chemicals were used without any further treatment or purification.

### 2.2 Characterization Techniques

The five zeolite samples were characterized by using XRD, ICP, FTIR, SEM, and BET surface area analysis. In details, XRD were acquired on a Bruker D2 PHASER benchtop, Massachusetts, USA, with CuK radiation, wavelength = 1.5418, to analyse the crystallinity of the zeolite samples. SEM analysis was used to examine the morphology of the investigated zeolite samples by using Jeol model 6360-LVSEM, USA. The exact concentration of Al in each zeolite sample was determined using ICP elemental analysis. The samples were digested before being microwaved for 90 min. The products of digestion were then passed through filters and washed multiple times. At last, the concentration of Al was determined using inductively coupled plasma optical emission spectroscopy, Thermo Scientific, ICAP 7000 series, component No: 1340910, Qtegra Software, Germany [32]. Using the  $\text{N}_2$  uptake data, the ultrastructural parameters of the fabricated catalyst samples (total surface area, pore size, and pore diameter) were determined. Nitrogen adsorption/desorption isotherms were obtained at 77 K on NOVA 2000e QuantaChrome instrument, Florida, USA. The pore size distribution was calculated using the Barret-Joyner-Halenda (BJH) model from the adsorption branch. Previously, the samples had been evacuated for 16 h at 623 K. The BET method was used to calculate the surface area ( $S_{\text{BET}}$ ) of the samples, while Lippens and Boer's t-plot method was used to estimate the pore volume ( $V_{\text{pore}}$ ). The produced catalytic samples were analysed using Fourier transform infrared (FTIR) spectroscopy on an Agilent Cary 630 FTIR Spectrometer, Santa Clara, California, USA. The spectra were taken at ambient conditions in the range 4000–400  $\text{cm}^{-1}$  with a spectral resolution of 4  $\text{cm}^{-1}$ .

### 2.3 Adsorption Study

The adsorption performance of different zeolites for the removal of MG dye was investigated using a batch procedure at room temperature. The dye solutions (100–200 mg/L) were prepared by diluting a stock MG solution (1000 mg/L) with distilled water. A UV–visible spectrophotometer (Double Beam, Shimadzu, 1800, Japan) was used to determine the initial and remaining concentration of MG dye in solutions at  $\lambda_{\max}$  of MG (i.e., 632 nm), which corresponds to the maximum absorption of MG. The various parameters that affect the adsorption percentage (%R) and adsorption capacity ( $q_e$ ), such as pH, temperature, contact time, adsorbent dosage, and initial concentration, were investigated. The parameters influencing the adsorption rate were investigated by altering one of the parameters while maintaining the others constant.

The percent of MG dye adsorption (%R) was determined by employing the equation:

$$\%R = \frac{(C_o - C_e)}{C_o} \times 100 \quad (1)$$

The amount of MG dye adsorbed at equilibrium per unit mass of adsorbent was determined according to the following equation:

$$q_e = (C_o - C_e) \cdot \frac{V}{m} \quad (2)$$

The adsorption capacity  $q_e$  in mg/g is equal to  $q_t$  at equilibrium, where  $q_t$  is the adsorption capacity (mg/g) at time  $t$ .

Where  $V$  is the volume of MG solution in (L), and ( $m$ ) the amount of adsorbent in (g),  $C_o$  and  $C_e$  are the initial concentration and equilibrium concentration (mg/L) of MG.

Moreover, to understand the adsorption mechanism of MG dye onto zeolites (HY, Beta and MOR), three different kinetic models (the pseudo-first-order model, the pseudo-second-order model, and the Elovich model) were employed to calculate the kinetic parameters. The following are the corresponding linear expressions of the kinetic equations:

$$\ln(q_e - q_t) = \ln q_e - k_1 t \quad (3)$$

$$\frac{t}{q_t} = \frac{1}{k_2 q_e^2} + \frac{t}{q_e} \quad (4)$$

$$q_t = \frac{1}{\beta} \ln(\alpha\beta) + \frac{1}{\beta} \ln t \quad (5)$$

where:

$k_1$  is the rate constant in the pseudo-first-order model,  $\text{min}^{-1}$

$k_2$  is the rate constant in the pseudo-second-order model,  $\text{g}/(\text{mg} \cdot \text{min})$ .

$\alpha$  is the initial adsorption rate  $\text{mg}/(\text{g} \cdot \text{min})$ .

$\beta$  is adsorption constant  $\text{g}/\text{mg}$ ,

Furthermore, the mechanism of transferring dye molecules from solutions to the solid surface of the absorbent material can be explained using the intra-particle diffusion model for Weber and Morris.

$$q_t = k_{\text{diff}} t^{1/2} + C \quad (6)$$

where  $k_{\text{diff}}$  is the intra-particle diffusion rate constant ( $\text{mg}/\text{g} \cdot \text{min}^{1/2}$ ) and  $C$  is a constant referring to the boundary layer width ( $\text{mg}/\text{g}$ ).

Given that there is no interaction between neighbouring adsorbed molecules and that adsorption sites have uniform energies, the Langmuir isotherm explains monolayer adsorption on a homogeneous surface. The linear forms of the Langmuir isotherm model can be represented as follows:

$$\frac{C_e}{q_e} = \frac{1}{K_L \cdot q_{\text{max}}} + \frac{C_e}{q_{\text{max}}} \quad (7)$$

Furthermore, the multilayer adsorption on the heterogeneous adsorbent surface is explained by the Freundlich isotherm.

$$\log q_e = \frac{1}{n} \log C_e + \log K_F \quad (8)$$

Another isotherm established by Dubinin and Radushkevich can be utilized to examine equilibrium data. It's used to calculate the mean free energy ( $E$ ) of adsorption, which is used to differentiate between chemical and physical adsorption.

$$\ln q_e = \ln q_{D-R} + \beta \varepsilon^2 \quad (9)$$

$$\varepsilon = RT \ln \left( 1 + \frac{1}{C_e} \right) \quad (10)$$

$q_{D-R}$ ,  $\beta$  and  $\varepsilon$  are adsorption capacity of MG ( $\text{mol}/\text{kg}$ ), the D–R constant ( $\text{mol}^2/\text{kJ}^2$ ) and the Polanyi potential respectively.

$\beta$  is the constant that is connected to the mean free energy ( $E$ ) of adsorption, which may be calculated using the given equations:

$$E = \frac{1}{\sqrt{2\beta}} \quad (11)$$

The thermodynamics of MG adsorption were studied using isotherms at four temperatures: 293, 303, 313 and 318 K. The following equations were used to evaluate the thermodynamic parameters.

$$\ln K_d = \frac{\Delta S}{R} - \frac{\Delta H}{RT} \quad (12)$$

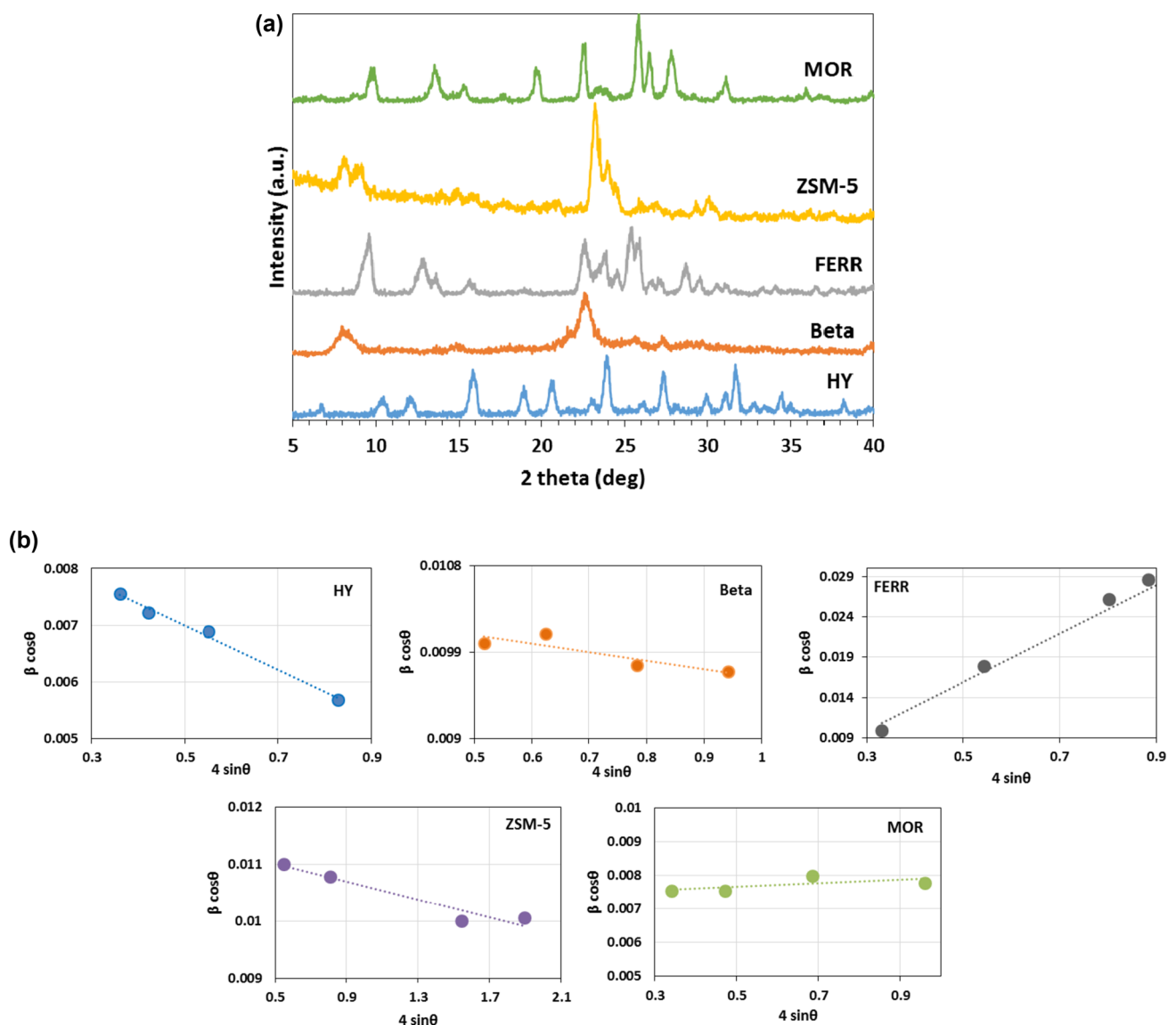
$$\Delta G^\circ = -RT \ln K_d \quad (13)$$

Where  $\Delta G$  is the free energy of adsorption (kJ/mol),  $R$  is the universal gas constant (J/mol·K),  $\Delta S$  is the entropy change (J/mol.K),  $\Delta H$  is the enthalpy change (kJ/mol),  $T$  is the temperature in Kelvin, and  $K_d$  is the thermodynamic equilibrium constant (dimensionless), whose values are calculated depending on the Langmuir constant ( $K_L$ ) [33]. The slope and intercept of a plot of  $\ln K_d$  vs.  $1/T$  could be used to determine  $H$  and  $S$ .

### 3 Results

#### 3.1 The Characterization of Zeolite Samples

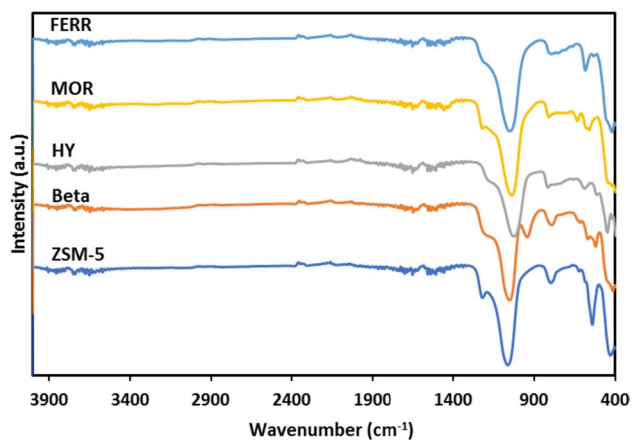
The degree of crystallization of zeolite samples was investigated by using the x-ray diffraction technique, the obtained patterns are plotted in Fig. 1. In general, all the investigated zeolites exhibited high crystallinity without any unknown phase(s), which reveals the high purity of the samples. MOR exhibited the peaks at  $9.77^\circ$ ,  $18.07^\circ$ ,  $20.34^\circ$ ,  $26.14^\circ$ ,  $28.89^\circ$ ,  $30.39^\circ$  and  $37.00^\circ$   $2\theta$ . These peaks can be referred to the lattice planes of (110), (200), (131), (041), (060), (441), and (531). This crystalline structure is matched with the indexed reference (JCPDS Card # 29–1257) [34]. ZSM-5



**Fig. 1** a The XRD diffractograms b Williamson-Hall (W-H) plots of the investigated zeolite samples

**Table 1** Estimated values of size ( $L$ ), dislocations ( $\delta$ ), strain ( $\epsilon_{\text{ave}}$ ), and x-ray density ( $\rho_{\text{x-ray}}$ ) for the investigated zeolite samples

Sample	Scherrer cal $L_{\text{ave}}$ (nm)	$\delta_{\text{ave}}$ (nm <sup>-2</sup> )	$\rho_{\text{x-ray}}$ (g/cm <sup>3</sup> )	$\epsilon_{\text{ave}}$
<b>HY</b>	99.90	0.0016	7.32	0.0124
<b>Beta</b>	13.99	4.9040	7.46	0.1606
<b>FERR</b>	77.11	0.0098	7.30	0.0210
<b>ZSM-5</b>	12.07	0.0074	7.38	0.0151
<b>MOR</b>	68.87	0.0016	7.36	0.0128

**Fig. 2** FTIR Spectra of the five investigated zeolite samples

sample exhibited peaks at 7.9°, 8.9°, 23.2°, and 24.0° which are assigned to the (101), (200), (501), and (303) planes of the MFI framework as indexed in the standard card number of JCPDS-44-0003) [35]. On the other hand, FERR sample exhibited the distinguished peaks which matched with the reference index of JCPDS file 98-007-5475. Beta sample exhibited two peaks at 7.6° and 22.4° which corresponding to the lattice planes of (101) and (302). According to the JCPDS 48-0038 cards, these peaks are relative to the BEA zeolite phase [36]. Finally, HY sample exhibited peaks which can be corresponding to the monoclinic planes of (002), (111), (200), (202), (202), (113), (311), (113) and

(220) as indexed in the reference of JCPDS:43-0168 [37]. The determined values of  $L$ ,  $\delta$ ,  $\epsilon$ ,  $\rho_{\text{x-ray}}$  and  $S$  are provided in Table 1.

FTIR analysis was performed on the five zeolite samples studied. Figure 2 shows the obtained spectra. Beta display two absorption bands at 525 and 575 cm<sup>-1</sup>, which are typical of the structure's five- and six-membered rings. The O-Si-O asymmetric stretching vibration is represented by the band around 1092 cm<sup>-1</sup> [38]. The spectrum of ZSM-5 revealed a strong band at 620 cm<sup>-1</sup>, which is the characteristic band of MFI-type zeolites with twice five rings' structures. HY [39] revealed that a band at 982 cm<sup>-1</sup> corresponds to the Si-O, SiO-Al, and Al-OH asymmetric and symmetric stretching vibrations that are associated with the internal TO<sub>4</sub> structure (T = Si, Al), whereas bands at 1146 and 790 cm<sup>-1</sup> correspond to the asymmetric and symmetric stretching vibrations associated to the external TO<sub>4</sub> structure (T = Si, Al), respectively. The band around 1389 cm<sup>-1</sup> corresponds with the Faujasite (FAU-type zeolite) structure's double-ring external link. Furthermore, vibrational stretches related to the Si-O group have been observed in MOR samples at 1040 cm<sup>-1</sup>. The wavelengths 800 cm<sup>-1</sup>, 550 cm<sup>-1</sup>, and 468 cm<sup>-1</sup> are associated with Al-O-Al vibrations, Si-O-Si vibrations, and internal asymmetric stretching of Al-O and Si-O [40].

The aluminium content in the five investigated zeolite samples was obtained from the producer. The highest aluminium content was found in HY sample (20wt% aluminium), while zeolite Beta contains the smallest aluminium content (only 0.33 wt%). In Table 2, the amount of aluminium as obtained from the producer is listed in the five investigated samples. One additional difference was also obtained from the producer, the counter cations in the framework. HY and Beta have protons (H<sup>+</sup>) as counter cations, while MOR, ZSM-5 and FERR have ammonium cations (NH<sub>4</sub><sup>+</sup>).

N<sub>2</sub> physisorption measurement was performed to measure the textural properties of the investigated zeolites. HY exhibited the highest surface area (720 m<sup>2</sup>/g), while the FERR exhibited the lowest surface area (only 400 m<sup>2</sup>/g). Surprisingly, the pore diameter of HY, Beta, and ZSM-5 was higher than 2 nm, which means that the pores in the three samples are in the range of mesoporous materials. Moreover, FERR

**Table 2** Textural properties of the investigated zeolite samples

Adsorbent	Al content (%)	Counter cation	Textural properties		
			Surface area (m <sup>2</sup> /g)	Pore volume (cm <sup>3</sup> /g)	Pore diameter (nm)
HY	20	H <sup>+</sup>	720	0.11	5.6
Beta	0.33	H <sup>+</sup>	615	0.23	4.8
MOR	5	NH <sub>4</sub> <sup>+</sup>	493	0.21	0.99
FERR	2	NH <sub>4</sub> <sup>+</sup>	400	0.19	1.1
ZSM-5	2	NH <sub>4</sub> <sup>+</sup>	420	0.24	5.9

and MOR have pore diameter in the range of microporous materials. The textural properties of the five investigated samples are listed in Table 1. Figure 3 shows the  $N_2$  isotherms of the five applied zeolite samples. HY and Beta samples showed the IV isotherms, which can be related to the mesoporous character according to IUPAC classification. On the other hand, MOR exhibited type III isotherm as an indication for the microporous character. However, ZSM-5 and FERR exhibited isotherms between type III and type IV, more investigation maybe required to explore this behaviour.

SEM analysis was used to investigate at the morphology of the five applied zeolite samples. Figure 4 displays the obtained micrographs. The five samples collectively shown substantial crystallization. HY displayed a crystalline phase with a few aggregates and partially duplicated octahedral crystals [41]. MOR showed merged aggregated prism-like crystals [42], while Beta showed sphere-like particle form [43]. Finally, ZSM-5 showed the hexagonal crystal structure of the aggregate [44].

### 3.2 The Adsorption Performance of Zeolite Samples

The adsorption performance of the five types of zeolites towards MG dye was tested and the adsorption capacities are shown in Fig. 5. For this comparison, 25 ml of MG solutions of different concentrations (100, 110, 120, 130, and

140 mg/l) were added to 0.05 g of each zeolite with stirring for 60 min. The results demonstrate that zeolite HY and MOR zeolites exhibited the highest MG dye removal. Furthermore, Beta came third after HY and MOR samples, and it exhibited higher adsorption capacity than ZSM-5 and FERR. The observed trend was true over the entire investigated MG concentrations. The adsorption capacity can be set in the order of  $HY \approx MOR > Beta > ZSM-5 > FERR$ . Based on the obtained results, the best performed three samples; HY, MOR, and Beta were chosen for the optimization study.

#### 3.2.1 Effect of Solution pH

The pH of the solution has a significant impact on the adsorbent and adsorbate properties. Therefore, the effect of pH on the adsorption percentage of MG onto the most performed zeolite samples; HY, Beta, and MOR was investigated over the pH range of 3–9. The pH was adjusted by using 0.1 M NaOH or 0.1 M HCl solutions. The effect of the pH was investigated through mixing 0.05 g of zeolite with 25 ml of MG solution (100 mg/L) and stirred at 600 rpm for 60 min. After that, the suspension was filtered to separate the zeolite sample from the solution. As seen in Fig. 6, it is observed that the MG adsorption percentage increases with increasing pH. It was found that the highest adsorbed amount of MG was at  $pH=9$ .

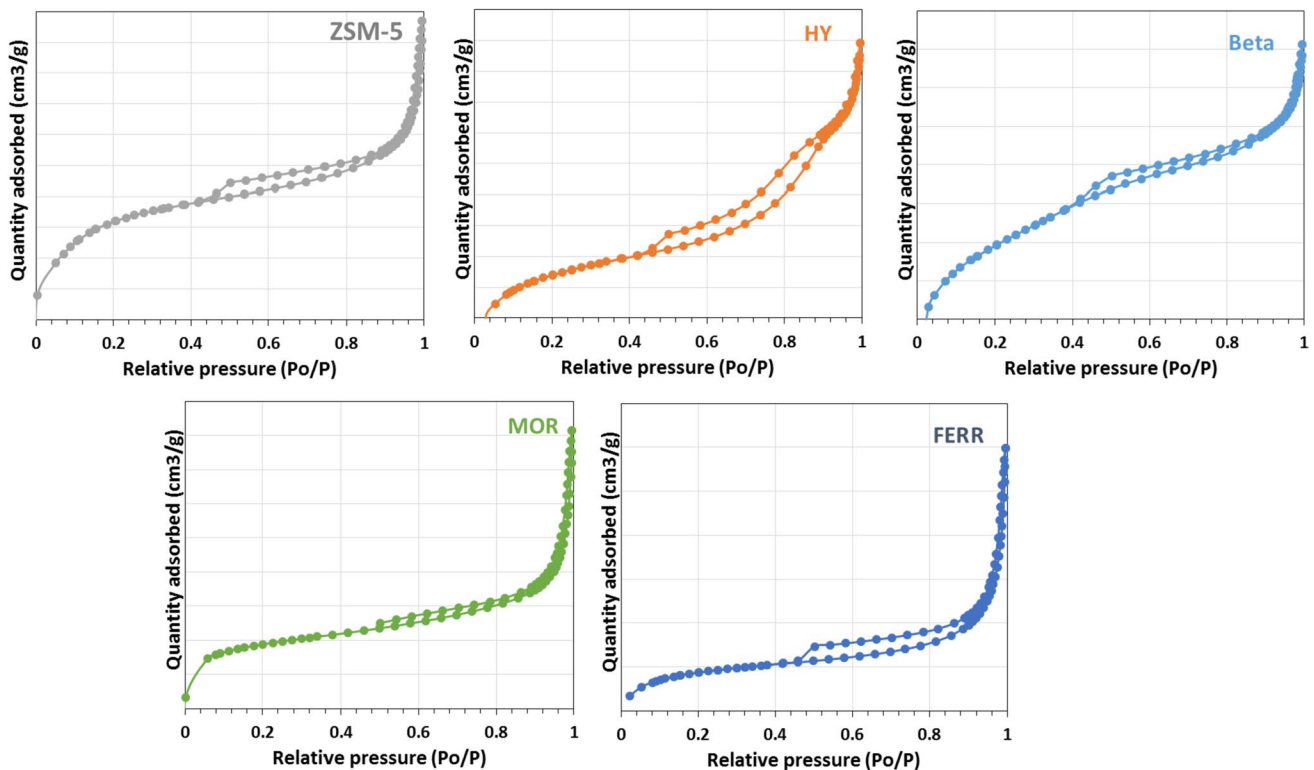


Fig. 3 The  $N_2$  isotherms of the zeolite samples as received from  $N_2$  adsorption/desorption measurements

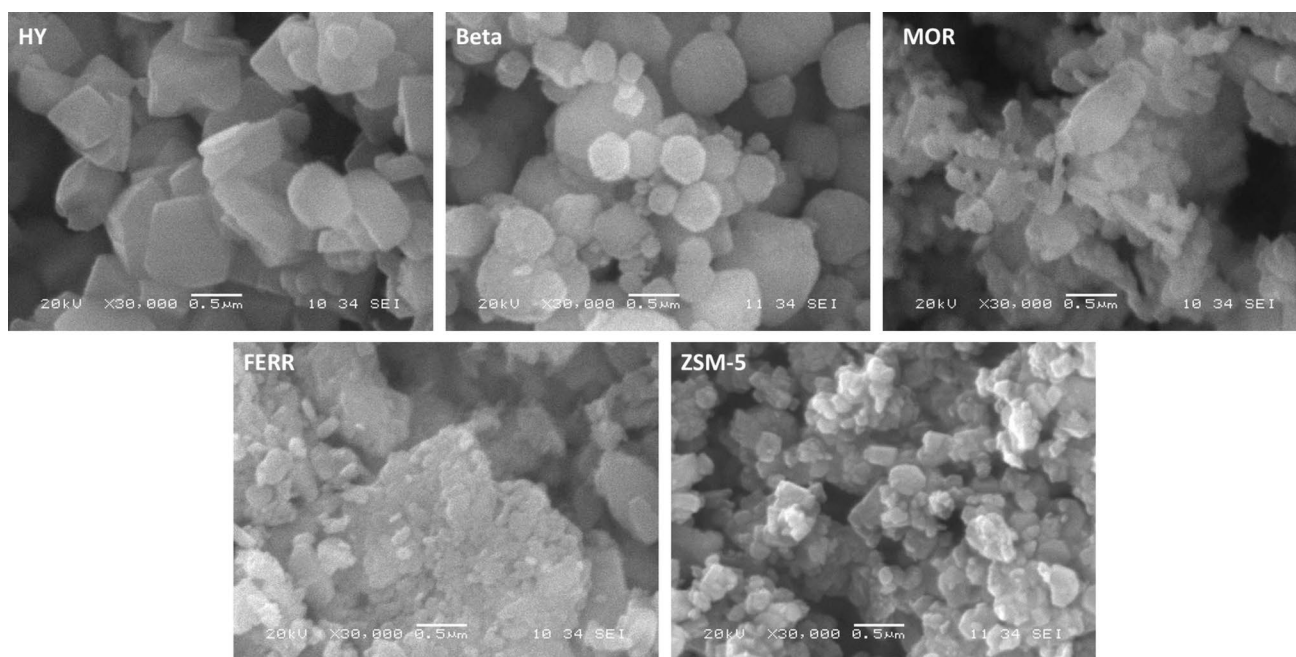


Fig. 4 SEM micrographs of the five investigated zeolite samples

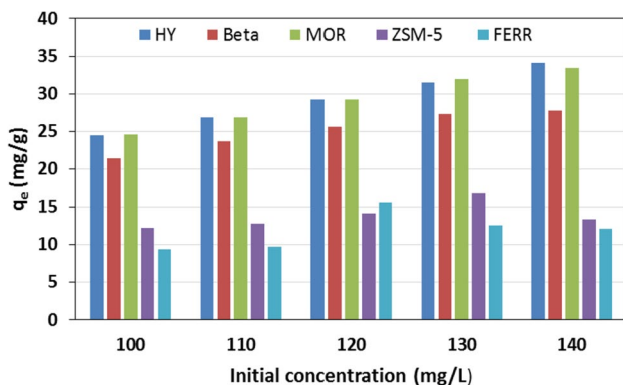


Fig. 5 The capacity of adsorption (mg/g) of MG dye over the different zeolite samples

This result agrees the reported results about the effect of pH on the adsorption of MG dye. Asim Khan et al. [45] reported that the best adsorption capacity was obtained at basic medium because at low pH, the excess of H<sup>+</sup> cations compete the dye molecules to adsorb faster on the surface of the adsorbent. Moreover, Tanaydina et al. [46] and Hamdy et al. [24] reported the same conclusion, and the best efficiency was obtained at basic medium.

### 3.2.2 Effect of Contact Time

Adsorption time is a significant parameter in adsorption investigations. The effect of contact time on MG adsorption was investigated by using time intervals ranging

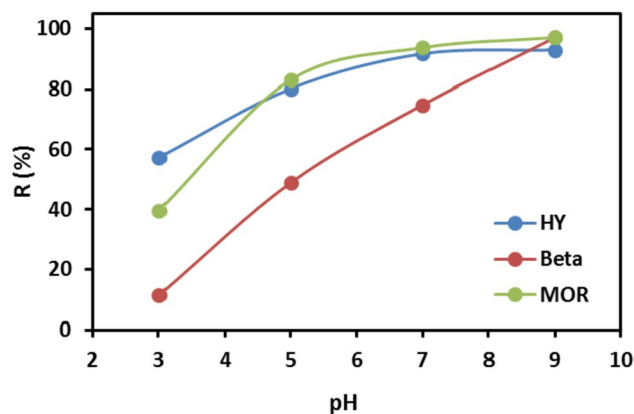
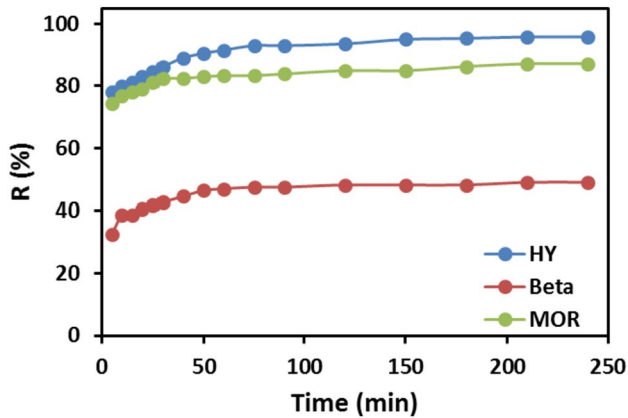


Fig. 6 Effect of initial pH solution on the adsorption percentage of MG dye. (Adsorption conditions: C<sub>0</sub> = 100 mg/L, adsorbent dosage = 2 g/L, time = 60 min, T = 298 K)

from 5 to 240 min. Figure 7 shows that the amount of MG adsorbed onto HY, Beta, and MOR zeolites nearly reached steady state in 60 min. Adsorption began with a linear rise, followed by a steady state. Therefore, 60 min was selected as the optimal contact time in subsequent experiments. The adsorption removal percentage (R, %) of MG were determined to be 91.58, 46.97 and 87.2% using HY, Beta and MOR, respectively.



**Fig. 7** The effect of contact time on adsorption percentage of MG dye. (Adsorption conditions:  $C_0=100$  mg/L, adsorbent dosage = 2 g/L,  $T=298$  K)

### 3.2.3 Effect of the Adsorbent Dosage

The adsorbent dosage for the adsorption studies were varied (0.02 to 0.1 g), keeping other parameters constant. The effects of adsorbent dosage on MG adsorption are presented in Fig. 8. The adsorption rate of MG increases gradually with the increase in the adsorbent amount. The removal percentage of MG dye increases from 79.5 to 97.8% by HY, from 19.8 to 85.7% by Beta, and from 59.1 to 98.3% by MOR, for an initial concentration of 100 mg/l. Typically, increasing the adsorbent dosage increases the percentage of dye removal, whereas increasing the adsorbent dose increases the number of sorption sites at the adsorbent surface. As a result, 0.1 g was chosen as the optimal dosage in subsequent experiments.

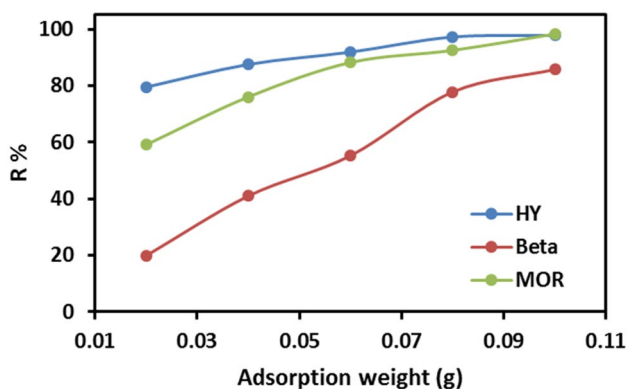


**Fig. 8** The effect of adsorbent dosage on adsorption percentage of MG (Adsorption conditions:  $C_0=100$  mg/L, time = 60 min,  $T=298$  K)

### 3.2.4 Effect of Initial Concentration

By generating an adsorbent-adsorbate solution with a fixed adsorbent dosage (0.1 g) and varied MG concentrations (100 to 200 mg/L) and whirling them together at room temperature for 60 min, one can test the influence of starting concentration. The initial dye concentration has a significant impact on the dye's rate of adsorption. The ratio of dye concentration to active binding sites on an adsorbent surface determines the impact of the initial concentration factor. Figure 9 shows how the percentage of dye removal decreases as the original dye concentration rises; this may be because the adsorption sites on the adsorbent surface are saturated.

### 3.2.5 Adsorption Kinetics

As shown in Table 3, the adsorption data is more fitted to the pseudo-second-order model based on the correlation coefficient ( $R^2$ ) values. The calculated values of  $q_e$  from the pseudo-second-order model (48.76 mg/g), (25.14 mg/g) and (44.84 mg/g) agree well with the experimental results (48.31 mg/g), (24.94 mg/g) and (43.59 mg/g), respectively. On the other hand, if the pseudo-first-order model is used, the experimental values of  $q_e$  are totally different.

The relation between adsorption capacity ( $q_t$ ) and time ( $t^{1/2}$ ) calculated from experimental data are shown in Fig. 10 (d). A linear approximation of the experimental data for HY, Beta and MOR zeolites gives two overlapping straight lines, which refer to two stages of MG diffusion on the zeolites. The kinetic parameters depicted in Table 4 were calculated using the second segment.

### 3.2.6 Isotherm Study

There are various isotherm models that can be used to explain the interaction between adsorbate and adsorbent.

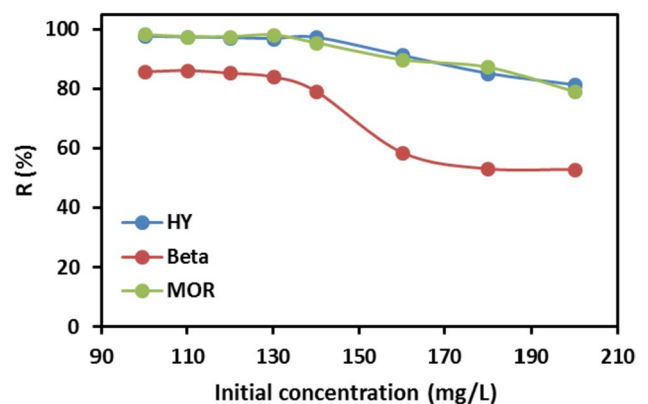


**Fig. 9** Effect of initial concentration on adsorption percentage of MG onto zeolites. (Adsorption conditions: adsorbent dosage = 4 g/L, time = 60 min,  $T=298$  K)



**Table 3** Kinetic parameters for the adsorption of MG

model	Adsorbent	HY	Beta	MOR
	$q_e$ experimental (mg/g)	47.96	24.52	43.59
Pseudo 1st model	$k_1$ ( $\text{min}^{-1}$ )	0.0202	0.0176	0.0122
	$q_e$ (mg/g)	8.756	5.033	4.746
	$R^2$	0.976	0.857	0.903
Pseudo 2nd model	$k_2$ (g/mg.min)	0.00601	0.00961	0.00634
	$q_e$ (mg/g)	48.54	24.88	44.84
	$R^2$	0.9999	0.9999	0.9896
Elovich model	$\alpha$ (mg/g.min)	$1.28 \times 10^6$	$2.53 \times 10^3$	$6.64 \times 10^9$
	$\beta$ (g/mg)	0.3818	0.4975	0.6326
	$R^2$	0.965	0.9254	0.9628

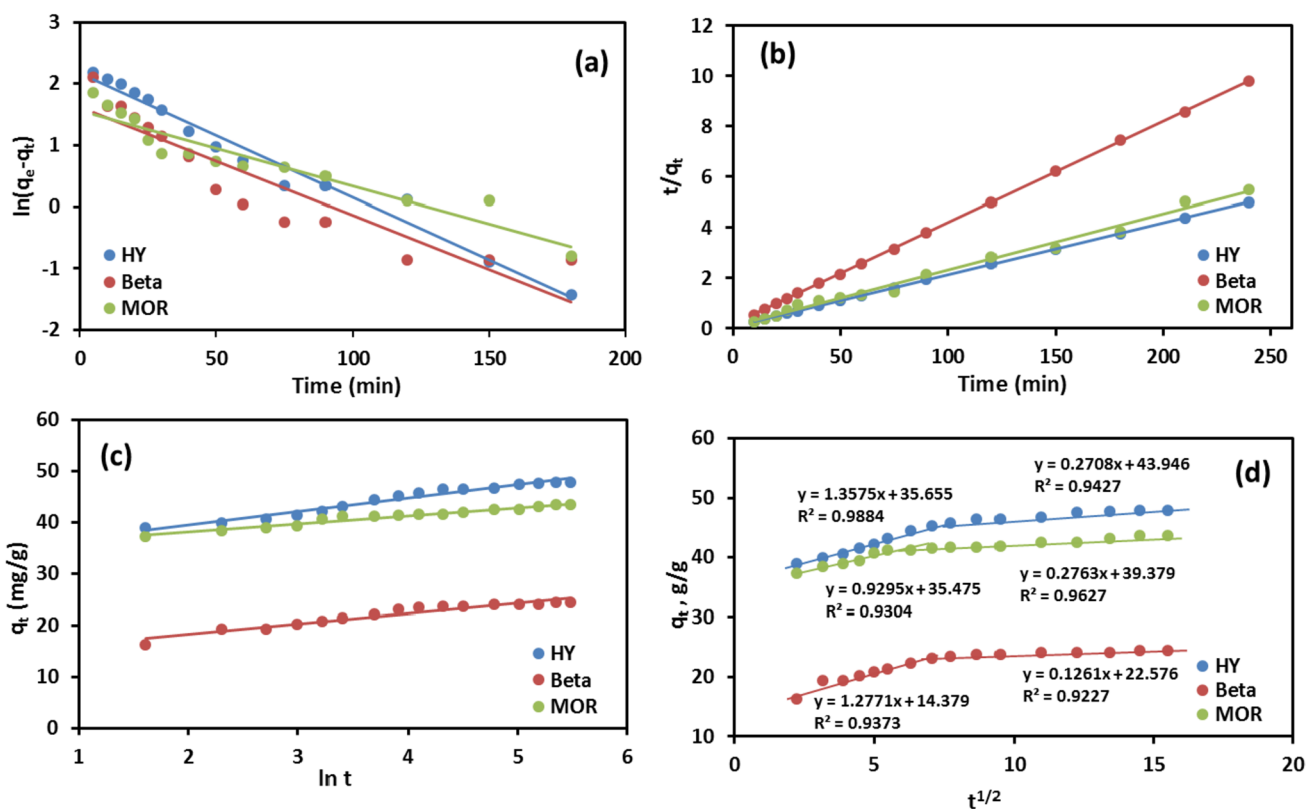


**Fig. 10** The kinetic models for MG adsorption onto HY, Beta and MOR zeolites as pseudo-first-order (a), pseudo-second-order (b), Elovich model (c), and intra-particle diffusion model (d)

**Table 4** The constants calculated from the intra-particle diffusion model

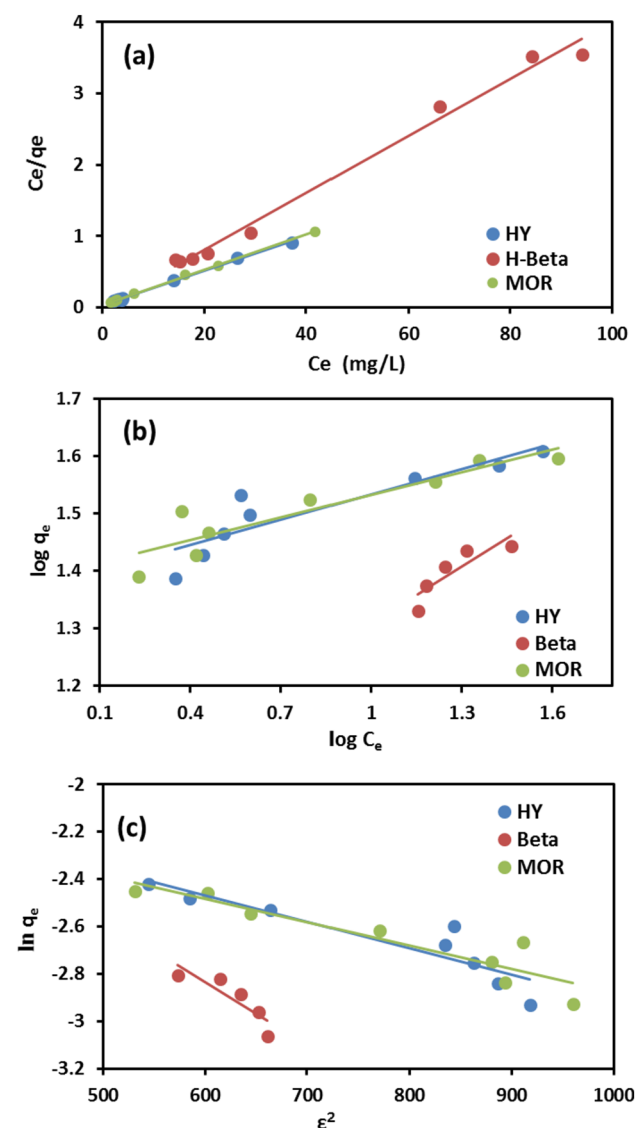
	HY	Beta	MOR
$k_{diff}$ (mg/g.min)	0.271	0.126	0.276
C (mg/g)	43.95	22.58	39.38
$R^2$	0.943	0.923	0.963

Langmuir, Freundlich, Dubinin-Radushkevich, and other isotherm models are examples. These isotherm models were investigated with various dye concentrations at constant pH, temperature, and adsorbent concentration.

As shown in Table 5 and Fig. 11 (a), the correlation coefficient ( $R^2 > 0.99$ ) indicates that the adsorption data are better fitted to the Langmuir adsorption model than the

**Table 5** Parameters of Langmuir, Freundlich, and Dubinin-Radushkevich equations for MG adsorption isotherms

Models	Parameters	HY	Beta	MOR
Langmuir model	$K_L$	0.699	4.707	0.846
	$q_m$ (mg/g)	41.54	25.05	40.57
	$R^2$	0.999	0.994	0.999
Freundlich model	$K_F$	24.37	9.618	25.16
	$1/n$	0.147	0.326	0.132
	$R^2$	0.904	0.871	0.918
Dubinin-Radushkevich (D-R) model	$q_{D-R}$ (mol /kg)	0.17	0.29	0.15
	$E$ (kJ/mol)	21.32	13.61	22.36
	$R^2$	0.8298	0.7671	0.8526

**Fig. 11** The linearized isotherms according to Langmuir (a), Freundlich (b) and Dubinin Radushkevich (c) models

Freundlich isotherm to explain the adsorption of MG on HY, Beta, and MOR.

### 3.2.7 Thermodynamic Study

The computed values of the thermodynamic parameters are displayed in Table 6. The  $G$  values in this study were all negative, demonstrating that the adsorption of MG onto various zeolites was spontaneous, which is enhanced by temperature. Additionally, the positive value of  $S$  indicates increased randomness at the solid–liquid interface during the adsorption process. Moreover, it was found that the enthalpy change value was positive when adsorbing MG over Beta, indicating endothermic adsorption. In contrast, in the adsorption of MG over zeolites HY and MOR, the  $\Delta H$  value was negative, indicating exothermic adsorption. (Fig. 12)

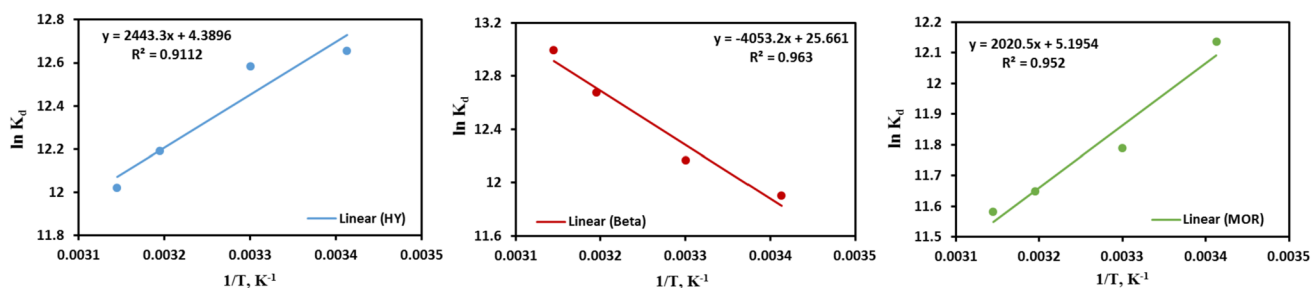
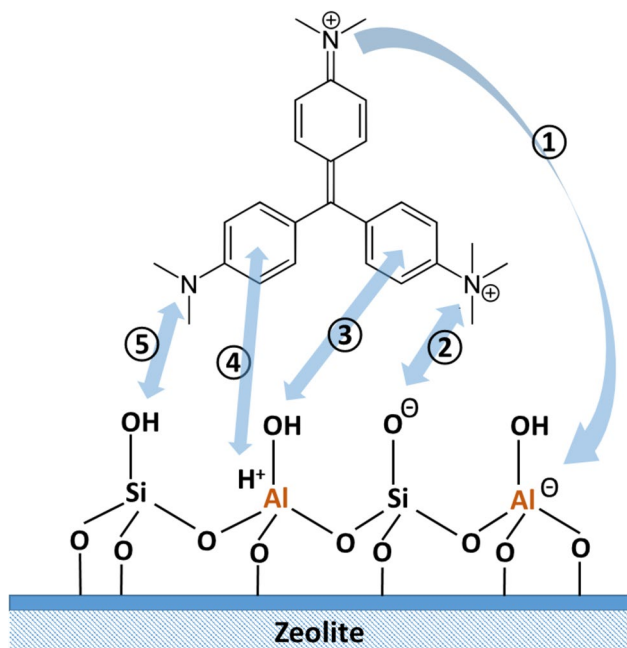
## 4 Discussion

### 4.1 The Proposed Adsorption Mechanism

As seen from the results, HY, Beta, and MOR exhibited the best adsorption performance. On the other hand, ZSM-5 and FERR showed less adsorption affinity towards MG dye. The explanation of the obtained results is not straight forward because several parameters are participating in the determination of the adsorption affinity. The parameters which affect the adsorption affinity are surface area, pore size, OH surface density, and Al content. MG undergoes ionization in water and two positive charge are locating on nitrogen atoms make it a perfect cationic dye. In zeolite, the replacement of  $Si^{4+}$  by  $Al^{3+}$  creates negative charge on Al atoms. These negative charges is permanent and cannot be removed, therefore,  $Al^{3+}$  ions which tetrahedrally coordinated in zeolite need counter cations (such as  $H^+$  or  $NH^+$ ) to neutralize the negative charge. Hence, the positive charges on nitrogen ions in the dye can strongly attracted to the negative charges on Al sites ① and also deprotonated silanol groups ② as seen in Fig. 13. Logically, as the number of  $Al^{3+}$  increases in the zeolite framework, more negative centres are formed, and more dye molecules can be adsorbed. This can explain why MOR is more active than Beta although Beta has high surface area than MOR, but it has very small Al content. On the other hand, another parameter must be considered, which is the repulsion between the adsorbed dye molecules on the zeolite surface. That is why there is no big difference between zeolite HY and MOR in adsorption capacity although HY has 4 times higher Al content. But repulsion force hindered the adsorption on the  $Al^{3+}$  rich surface. As reported in the study of Hartanto et al. [47], another medium attraction can promote the adsorption of organic dyes over zeolite, which is the attraction between the delocalised  $\pi$  electron in dye

**Table 6** The thermodynamic parameters for adsorption of MG onto HY, Beta, and MOR

HY	T, °C	T,K	1/T	KL	Kd	ln Kd	Slope	Intercept	$\Delta H$	$\Delta S$	$\Delta G$
	20	293	0.00341	0.682927	313,101.5	12.6543	2443.3	4.3896	-20.31	36.50	-30.83
	30	303	0.00330	0.635514	291,364.1	12.5823	2443.3	4.3896			-31.70
	40	313	0.00319	0.429577	196,948.4	12.1907	2443.3	4.3896			-31.72
	45	318	0.00314	0.363057	166,450.9	12.0225	2443.3	4.3896			-31.79
Beta	T, °C	T,K	1/T	KL	Kd	ln Kd	Slope	Intercept	$\Delta H$	$\Delta S$	$\Delta G$
	20	293	0.00341	0.321918	147,589.7	11.9022	-4053	25.661	33.70	213.35	-28.99
	30	303	0.00330	0.418994	192,096.4	12.1658	-4053	25.661			-30.65
	35	308	0.00325	0.656098	300,801	12.6142	-4053	25.661			-32.30
	45	318	0.00314	0.957895	439,166	12.9926	-4053	25.661			-34.35
MOR	T, °C	T,K	1/T	KL	Kd	ln Kd	Slope	Intercept	$\Delta H$	$\Delta S$	$\Delta G$
	20	293	0.00341	0.406504	186,369.9	12.1355	2020.5	5.1954	-16.80	43.19	-29.56
	30	303	0.00330	0.287197	131,671.3	11.7881	2020.5	5.1954			-29.70
	40	313	0.00319	0.25	114,617.5	11.6494	2020.5	5.1954			-30.31
	45	318	0.00314	0.233728	107,157.2	11.5821	2020.5	5.1954			-30.62

**Fig. 12**  $\ln K_d$  versus  $1/T$  plots for MG adsorption on zeolites (HY, Beta, and MOR)**Fig. 13** The proposed mechanism of MG adsorption over the different zeolite samples

benzene ring and the hydrogen atoms in the adsorbents ③ and ④. This can explain the high adsorption of zeolite Beta which has hydrogen ions as a counter cations for the small  $Al^{3+}$  content. Finally, hydrogen bonding ⑤ can play a role in the adsorption affinity of the zeolite samples. In addition to the high surface area and the wide pore volume which offers high accessibility to dye molecules to travel inside the pores of the crystals. These two factors gave advantage for Beta over FERR and ZSM-5.

## 4.2 Activity comparison

Several studies were performed to investigate the efficiency of different adsorbents in the removal of MG dye. The adsorption capacity (mg/g) for the different adsorbents from literature is compared with that of commercial zeolites of the current study in Table 7.

The data listed in Table 7 shows that the zeolite samples can work in an efficient way as good adsorbents in the removal of MG dye. HY exhibited the second best adsorption capacity after the activated carbon samples. Moreover, HY and MOR exhibited better efficiency than three siliceous

**Table 7** A comparison between the adsorption capacity (mg/g) for the different adsorbents from literature with that of commercial zeolites of the current study

Category	Adsorbent	Adsorption capacity (mg/g)	References
Siliceous mesoporous materials	SBA-S4	39.4	[48]
	MCM-41	20.9	[49]
	TUD-1	14.0	[24]
Metal organic framework	MOF [Mn <sub>4</sub> (L) <sub>2</sub> (H <sub>2</sub> O) <sub>4</sub> ] <sub>n</sub> ·4DMF·H <sub>2</sub> O	25.8	[50]
	MOF with [Zn <sub>4</sub> O] Clusters	3.45	[51]
Bio-based adsorbents	Almond shell	1.10	[52]
	Bamboo	20.4	[53]
	Saccharomyces cerevisiae	20.1	[54]
	Activated carbon	67.9	[55]
	Activated carbon	71.4	[56]
	graphite oxide	29.4	[57]
	graphite oxide	28.5	-
Zeolites	HY	41.5	This study
	Beta	25.1	This study
	MOR	40.6	This study

mesoporous materials and two reported MOF samples. The listed data opens a new window for further improvement in zeolite samples to be the best synthetic adsorbent for cationic dyes.

## 5 Conclusion

The commercially available zeolite materials have significant differences such as morphological structure, textural properties, aluminium ratio, and the counter cation. Due to such differences, there is a remarkable difference in adsorption affinity of the zeolite samples. The current study pointed out to the great variation in the adsorption affinity of zeolite samples towards the cationic MB dye. The Al content plays the important factor in the adsorption affinity towards the investigation dye. While surface area and the pore diameter showed also significant effect on the adsorption affinity. However, the counter cation in zeolite framework did not show a major effect on zeolite adsorption of cationic dye. The samples HY, Beta, and MOR exhibited the most adsorption affinity towards MG dye. HY and MOR showed very similar behaviour, however, Beta exhibited different mechanism most likely due to the very small content of Al ions. The overall adsorption process was found to be spontaneous endothermic process over Beta sample, while it was spontaneous exothermic over HY and MOR. Moreover, the adsorption process belongs to the physical type with a monolayer coverage.

**Acknowledgements** The authors extend their appreciation to the Deanship of Scientific Research at King Khalid University for funding this work through large group Research Project under grant number RGP2/236/44

**Author contributions** F.A.I. and A.A.A. performed the experimental study and M.S.H. wrote the manuscript and supervised the entire work

**Funding** The current research was funded from the Deanship of Scientific Research at King Khalid University for funding this work through large group Research Project under grant number RGP2/236/44.

**Data Availability** The data of the current research are available upon request from the corresponding author.

## Declarations

**Conflict of interest** The author declare no conflict of interest.

**Ethical approval** Not applicable.

**Consent to participate** Not applicable.

**Consent for publication** Authors of the current manuscript are agree to publish it in the current form.

## References

1. N. Akhtar, M. I. Syakir Ishak, S. A. Bhawani, K. Umar, Various natural and anthropogenic factors responsible for water quality degradation: A review. *Water*. **13**(19), 2660(2021).
2. N Chaukura KK Kefeni I Chikurunhe I Nyambiya W Gwenzi W Moyo FO Abulude 2021 Microplastics in the aquatic environment—the occurrence, sources, ecological impacts, fate, and remediation challenges *Pollutants*. 1 2 95 118
3. A Tkaczyk K Mitrowska A Posyniak 2020 Synthetic organic dyes as contaminants of the aquatic environment and their implications for ecosystems: A review *Sci. Total Environ.* 717 137222
4. A Sridhar M Ponnuchamy A Kapoor S Prabhakar 2022 Valorization of food waste as adsorbents for toxic dye removal from contaminated waters: A review *J. Hazard. Mater.* 424 127432
5. A Saravanan PS Kumar S Jeevanantham S Karishma B Tajsabreen PR Yaashikaa B Reshma 2021 Effective water/wastewater

- treatment methodologies for toxic pollutants removal: Processes and applications towards sustainable development *Chemosphere* 280 130595
- OJ Hao H Kim PC Chiang 2000 Decolorization of wastewater *Crit. Rev. Environ. Sci. Technol.* 30 4 449 505
  - IK Kapdan F Kargi 2002 Simultaneous biodegradation and adsorption of textile dyestuff in an activated sludge unit *Process Biochem.* 37 9 973 981
  - EG Solozhenko NM Soboleva VV Goncharuk 1995 Decolorization of azodye solutions by Fenton's oxidation *Water Res.* 29 9 2206 2210
  - KR Prasad 2009 Color removal from distillery spent wash through coagulation using *Moringa oleifera* seeds: Use of optimum response surface methodology *J. Hazard. Mater.* 165 1–3 804 811
  - M Panizza A Barbucci R Ricotti G Cerisola 2007 Electrochemical degradation of methylene blue *Sep. Purif. Technol.* 54 3 382 387
  - AC Buckley 1992 Membrane technology for the treatment of dye-house effluents *Water Sci. Technol.* 25 10 203
  - D. M. EL-Mekkawi, F. M. Ibrahim, M.M. Selim, Stability and thermal transformation studies of  $Zn^{2+}$ - and  $Fe^{2+}$ -loaded zeolite Y prepared from Egyptian kaolin. *Solid State Sciences.* 48, 294–299(2015).
  - D. M. EL-Mekkawi, F. M. Ibrahim, M.M. Selim, Removal of methylene blue from water using zeolites prepared from Egyptian kaolins collected from different sources. *Journal of Environmental Chemical Engineering.* 4(2), 1417–1422 (2016).]
  - Y. D. Ngapa, S. Sugiarti, Z. Abidin, Z. Hydrothermal transformation of natural zeolite from Ende-NTT and its application as adsorbent of cationic dye. *Indonesian Journal of Chemistry.* 16(2), 138–143 (2016).
  - M. M. Selim, D. M. EL-Mekkawi, F. M. Ibrahim, Innovative synthesis of black zeolites-based kaolin and their adsorption behavior in the removal of methylene blue from water. *Journal of Materials Science.* 53, 3323–3331(2018).
  - J. Wiley, Ullmann's Encyclopedia of Industrial Chemistry. 27 (2001).]
  - BG Berg DM Green 1990 Spectral weights in profile listening *The Journal of the Acoustical Society of America.* 88 2 758 766
  - T Geethakrishnan PK Palanisamy 2006 Degenerate four-wave mixing experiments in Methyl green dye-doped gelatin film *Optik* 117 6 282 286
  - W Huang J Jia Z Zhang X Han J Tang J Wang E Wang 2003 Hydrogen peroxide biosensor based on microperoxidase-11 entrapped in lipid membrane *Biosens. Bioelectron.* 18 10 1225 1230
  - Q Li H Liu Y Wang Z Sun F Guo J Zhu 2014 Methyl green and nitrotetrazolium blue chloride co-expression in colon tissue: A hyperspectral microscopic imaging analysis *Opt. Laser Technol.* 64 337 342
  - A. Belgacem, I. Ould Brahim, M. Belmedani, H. Hadoun, Removal of methyl green dye from aqueous solutions using activated carbon derived from cryogenic crushed waste tires. *Iranian Journal of Chemistry and Chemical Engineering.* 41(1), 207–219 (2022).]
  - NM Mahmoud MM El-Moselhy MA Alkhalidi 2019 Remediation of methyl green dye from aqueous solution via adsorption and degradation using silica gel modified with hydrated zinc oxide catalyst *Desalin. Water Treat.* 158 385 397
  - Y. Satlaoui, M. Trifi, D. Fkih Romdhane, A. Charef, R. Azouzi, Removal properties, mechanisms, and performance of methyl green from aqueous solution using raw and purified sejnane clay type. *Journal of Chemistry.* (2019).
  - BM Al-Shehri SK Mohamed S Alzahly MS Hamdy 2021 A significant improvement in adsorption behavior of mesoporous TUD-1 silica through neodymium incorporation *J. Rare Earths* 39 4 469 476
  - RW Schurko MJ Jaroszewicz 2015 Solid-state NMR of the light main group metals *The Lightest Metals Encyclopedia of Inorganic and Bioinorganic Chemistry* 117 172
  - B Jha DN Singh 2011 A review on synthesis, characterization and industrial applications of flyash zeolites *J. Mater. Educ.* 33 1 65
  - C Miranda J Urresta H Cruchade A Tran M Benghalem A Astafan L Pinard 2018 Exploring the impact of zeolite porous voids in liquid phase reactions: The case of glycerol etherification by tert-butyl alcohol *J. Catal.* 365 249 260
  - Y Li J Yu 2021 Emerging applications of zeolites in catalysis, separation and host-guest assembly *Nat. Rev. Mater.* 6 12 1156 1174
  - H Ramezani SN Azizi G Cravotto 2019 Improved removal of methylene blue on modified hierarchical zeolite Y: Achieved by a “destructive-constructive” method *Green Processing and Synthesis.* 8 1 730 741
  - A Imessaoudene S Cheikh JC Bollinger L Belkhiri A Tiri A Bouzaza L Mouni 2022 Zeolite waste characterization and use as low-cost, ecofriendly, and sustainable material for malachite green and methylene blue dyes removal: Box-behken design, kinetics, and thermodynamics *Appl. Sci.* 12 15 7587
  - AR Gollakota VS Munagapati SW Liao CM Shu KP Shadangi PK Sarangi JC Wen 2023 Ionic liquid [bmim][TFSI] templated Na-X zeolite for the adsorption of  $(Cd^{2+}, Zn^{2+})$ , and dyes (AR, R6) *Environ. Res.* 216 114525
  - Orsikowsky-Sanchez, A.; C. Franke, A. Sachse, E. Ferrage, S. Petit, J. Brunet, F. Plantier, C. Miqueu. *Nanomaterials* 11 (2021) 1205.
  - E. C. Lima, A. Hosseini-Bandegharai, J. C. Moreno-Piraján, I. Anastopoulos, A critical review of the estimation of the thermodynamic parameters on adsorption equilibria. Wrong use of equilibrium constant in the Van't Hoof equation for calculation of thermodynamic parameters of adsorption. *Journal of molecular liquids.* 273, 425–434 (2019).
  - H Smail K Shareef Z Ramli 2017 Synthesis of mesoporous mor-denite zeolite by different natural raw materials *Aust J Basic App Sci.* 11 27 34
  - J Wang J Shan Y Tian T Zhu H Duan X He G Liu 2021 Catalytic cracking of n-heptane over Fe modified HZSM-5 nanosheet to produce light olefins *Fuel* 306 121725
  - B Ray C Matter 1995 Solid catalysts and porous solids Structure and characterization of catalysts Related review: Recent developments in *Condens Matter.* 51 2805 3281
  - R. Shoja Razavi, M. R. Loghman-Estarki, Synthesis and characterizations of copper oxide nanoparticles within zeolite Y. *Journal of Cluster Science.* 23, 1097–1106 (2012).]
  - J Li H Liu T An Y Yue X Bao 2017 Carboxylic acids to butyl esters over dealuminated–realuminated beta zeolites for removing organic acids from bio-oils *RSC Adv.* 7 54 33714 33725
  - A. Mekki, A. Benmaati, A. Mokhtar, M. Hachemaoui, F. Zaoui, H. Habib Zahmani, B. Boukoussa, Michael addition of 1, 3-dicarbonyl derivatives in the presence of zeolite Y as an heterogeneous catalyst. *Journal of Inorganic and Organometallic Polymers and Materials.* 30, 2323–2334 (2020).
  - MA Klunk SB Schröpfer S Dasgupta M Das NR Caetano AN Impiombato CAM Moraes 2020 Synthesis and characterization of mor-denite zeolite from metakaolin and rice husk ash as a source of aluminium and silicon *Chem. Pap.* 74 2481 2489
  - S Ye J Sun X Yi Y Wang Q Zhang 2017 Interaction between the exchanged  $Mn^{2+}$  and  $Yb^{3+}$  ions confined in zeolite-Y and their luminescence behaviours *Sci. Rep.* 7 1 46219
  - H. M. Hussain, A. A. K. Mohammed, Preparation and characterization of mor-denite zeolite from iraqi sand. In *IOP Conference Series: Materials Science and Engineering.* 518, 062002 (2019).
  - Z Huang JF Su YH Guo XQ Su LJ Teng 2009 Synthesis of well-crystallized zeolite beta at large scale and its incorporation into

- polysulfone matrix for gas separation *Chem. Eng. Commun.* 196 9 969 986
44. H. Reza Safaei, M. Reza Safaei, V. Rahmanian, Film formation and anticorrosive behavior of Zn-ZSM-5 nano-sized zeolite composite coatings. *The Open Electrochemistry Journal.* **4(1)** (2012).
  45. M Ikram S Mutahir M Humayun MA Khan JY Al-Humaidi MS Refat AS Abouzied 2022 Facile Synthesis of ZIF-67 for the Adsorption of Methyl Green from Wastewater: Integrating Molecular Models and Experimental Evidence to Comprehend the Removal Mechanism *Molecules* 27 23 8385
  46. MK Tanaydin A Goksu 2021 Optimization of the adsorption of methyl green dye on almond shells using central composite design *Desalination Water Treat* 227 425 439
  47. A Iryani A Masudi AI Rozafia D Hartanto M Santoso H Nur MS Azami 2020 Enhanced removal of soluble and insoluble dyes over hierarchical zeolites: Effect of synthesis condition *Inorganics* 8 9 52
  48. L Arjomandi-Behzad MK Rofouei A Badiie JB Ghasemi 2022 Simultaneous removal of crystal violet and methyl green in water samples by functionalised SBA-15 *Int. J. Environ. Anal. Chem.* 102 17 5919 5935
  49. S. M. Alardhi, T. M. Albayati, J. M. Alrubaye, Adsorption of the methyl green dye pollutant from aqueous solution using mesoporous materials MCM-41 in a fixed-bed column. *Heliyon*, **6(1)**, (2020).
  50. S Cheng Y Wu J Jin J Liu D Wu G Yang YY Wang 2019 New multifunctional 3D porous metal-organic framework with selective gas adsorption, efficient chemical fixation of CO<sub>2</sub> and dye adsorption *Dalton Trans.* 48 22 7612 7618
  51. KP Bai LJ Zhou GP Yang MX Cao YY Wang 2020 Four new metal-organic frameworks based on diverse metal clusters: Syntheses, structures, luminescent sensing and dye adsorption properties *J. Solid State Chem.* 287 121336
  52. MK Tanaydin A Goksu 2021 Optimization of the adsorption of methyl green dye on almond shells using central composite design *Desalination Water Treat.* 227 425 439
  53. AA Atshan 2014 Adsorption of methyl green dye onto bamboo in batch and continuous system *Iraqi Journal of Chemical and Petroleum Engineering.* 15 1 65 72
  54. MS Al-Tameemi M Mohammed AAT Al-Sadoon 2022 Study the ability of *Saccharomyces cerevisiae* to remove methyl green dye from water as a pollutant agent *Journal of Chemical Health Risks* 12 1 93 104
  55. K. Rida, K. Chaibeddra, K. Cheraitia, Adsorption of cationic dye methyl green from aqueous solution onto activated carbon prepared from brachyichitonpopulneus fruit shell. (2020).
  56. AA Farghali M Bahgat WMA Roubay El MH Khedr 2013 Preparation, decoration and characterization of graphene sheets for methyl green adsorption *J. Alloy. Compd.* 555 193 200
  57. P Sharma BK Saikia MR Das 2014 Removal of methyl green dye molecule from aqueous system using reduced graphene oxide as an efficient adsorbent: Kinetics, isotherm and thermodynamic parameters *Colloids Surf., A* 457 125 133

**Publisher's Note** Springer Nature remains neutral with regard to jurisdictional claims in published maps and institutional affiliations.

Springer Nature or its licensor (e.g. a society or other partner) holds exclusive rights to this article under a publishing agreement with the author(s) or other rightsholder(s); author self-archiving of the accepted manuscript version of this article is solely governed by the terms of such publishing agreement and applicable law.